Journal of Power Sources 221 (2013) 84–89

Contents lists available at SciVerse ScienceDirect

Journal of Power Sources

journal homepage: www.elsevier.com/locate/jpowsour

Effect of annealing on the structure and electrochemical properties of $La_{1.8}Ti_{0.2}MgNi_{8.9}Al_{0.1}$ hydrogen storage alloy

Weiqing Jiang [a,*], Xiaohua Mo [b], Jin Guo [a,*], Yinyan Wei [a]

[a] Key Laboratory of National Education Ministry for Nonferrous Metals and Materials Processing Technology, College of Physics Science and Technology, Guangxi University, Nanning 530004, China
[b] Faculty of Science, Guangxi University for Nationalities, Nanning 530006, China

HIGHLIGHTS

- As-cast and annealed $La_{1.8}Ti_{0.2}MgNi_{8.9}Al_{0.1}$ alloys are prepared.
- After annealing, the composition becomes homogenous.
- Suitable annealing markedly improves cycle life and high rate dischargeability.
- The most appropriate annealing temperature for the alloy studied is 900 °C.

GRAPHICAL ABSTRACT

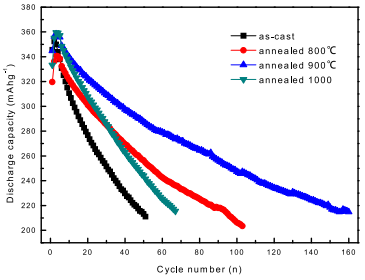

ARTICLE INFO

Article history:
Received 3 June 2012
Received in revised form
16 July 2012
Accepted 9 August 2012
Available online 17 August 2012

Keywords:
Hydrogen storage alloy
Annealing
Microstructure
Electrochemical property

ABSTRACT

$La_{1.8}Ti_{0.2}MgNi_{8.9}Al_{0.1}$ alloys have been prepared by magnetic levitation melting followed by annealing treatment. The effects of annealing on the structure and electrochemical properties of the alloys are investigated by XRD, SEM–EDS and electrochemical measurement. For as-cast and annealed $La_{1.8}Ti_{0.2}MgNi_{8.9}Al_{0.1}$ alloys, $La(Ni,Al)_5$ and $LaMg_2Ni_9$ are the main phases. Annealing not only causes $LaNi_2$ phase to disappear, but also brings higher compositional homogeneity, which contributes to the improvement of cycling stability. At 60% discharge capacity retention, the maximum charge–discharge cycles, 160 cycles (at 900 °C), is more than three times the minimum, 51 cycles (as-cast). The positive impact of annealing (at 800 °C and 900 °C) on the charge transfer rate at the surface and the hydrogen diffusion rate in the bulk enhances the HRD. The optimum annealing temperature is found to be 900 °C.

1. Introduction

After a series of AB_3-type La-Mg-Ni-based alloys was reported by Kadir et al. [1], great efforts have been focused on developing the La–Mg–Ni-based alloys ($AB_{3-3.8}$-type) as hydrogen storage materials, and great progresses have been achieved. High electrochemical capacities around 400 mAh g^{-1} have been reported for series of La–Mg–Ni-based alloys, which is about 25% higher than that of the AB_5-type alloys [2–5]. However, the significant oxidation and pulverization during charge/discharge process in the KOH aqueous solution is the main obstacle for the practical application of the La–Mg–Ni-based alloys. It is well known that annealing treatment is a very effective way to improve the overall hydrogen storage properties, such as hydrogen storage capacity, discharge capacity, cyclic stability, high rate dischargeability, and so on [6–10]. Sakai et al. [6] reported that annealing treatment could decrease the crystal defects and increase alloy composition homogenization, and consequently enhance the discharge capacity and cyclic life of the rare-earth-based hydrogen storage alloys. Pan et al. [7] revealed that annealed $La_{0.7}Mg_{0.3}Ni_{2.45}Co_{0.75}Mn_{0.1}Al_{0.2}$ alloys exhibited larger discharge capacity and longer cycle life

* Corresponding authors. Tel.: +86 771 3237386.
E-mail addresses: wqjiang@gxu.edu.cn (W. Jiang), guojin@gxu.edu.cn (J. Guo).

0378-7753/$ – see front matter © 2012 Elsevier B.V. All rights reserved.
http://dx.doi.org/10.1016/j.jpowsour.2012.08.022

compared to as-cast alloy owing to the variable phase abundance and composition homogenization, respectively. Zhang et al. [8] found that for $La_{0.67}Mg_{0.33}Ni_{2.5}Co_{0.5}$ alloy, after annealing treatment, the absorption/desorption plateau became flatter and wider, and the discharge capacity and cyclic stability were all improved. Huang et al. [9] showed that annealing improved the hydrogen absorption and desorption plateau performance, and increased the reversible hydrogen storage capacity of $La_{0.78}Mg_{0.22}Ni_{3.48-}Co_{0.22}Cu_{0.12}$ alloy. Recently, we have studied the effects of annealing on the hydrogen storage properties of La–Ti–Mg–Ni alloys, and found that heat treatment not only reduced the desorption plateau pressure, enhanced the hydrogen storage capacity and discharge capacity, but also prolonged the cycle life [10].

In this present study, annealing treatment was employed in $La_{1.8}Ti_{0.2}MgNi_{8.9}Al_{0.1}$ alloy so as to improve its electrochemical characteristics, and the effect of annealing on the structure and electrochemical characteristics of as-cast and annealed $La_{1.8}Ti_{0.2}MgNi_{8.9}Al_{0.1}$ alloys were studied in detail.

2. Experimental

$La_{1.8}Ti_{0.2}MgNi_{8.9}Al_{0.1}$ alloy was prepared by magnetic levitation melting under argon atmosphere followed by annealing treatments at 800 °C, 900 °C and 1000 °C for 10 h under vacuum. The purity of starting elemental metals was higher than 99.9%.

The crystal components of each sample were checked by X-ray powder diffraction (XRD) on a Rigaku D/max 2500 V diffractometer with Cu Kα radiation. The lattice parameters and cell volumes were analyzed by the Materials Data Inc. software Jade 5.0 and a Powder Diffraction File (PDF release 2002). The morphology and elemental composition of the ingot samples were investigated by used scanning electron microscope (SEM, HITACHI S-3400N) equipped with energy dispersive spectrometer (EDS) analysis.

The hydride electrode was prepared by cold pressing the mixture of alloy powder (200 mesh) and carbonyl nickel powder in a weight ratio of 1:4 to form a pellet under a pressure of 25 MPa. Electrochemical measurements were performed in a standard open tri-electrode electrolysis cell, consisting of a metal hydride electrode, a sintered $Ni(OH)_2$/NiOOH counter electrode and a Hg/HgO reference electrode immersing in 6 M KOH electrolyte. The electrochemical activation and cyclic stability were measured using an automatic DC-5 battery testing instrument. The test electrodes were charged at 100 mA g^{-1} for 5 h followed by a rest of 10 min, and then discharged at 80 mA g^{-1} to a cut-off cell potential of −0.5 V (versus the Hg/HgO reference electrode). The high rate dischargeability (HRD) was carried out at different current densities using an Arbin instrument. The linear polarization curves were measured on Gamry instrument by scanning electrode potential at the rate of 0.1 mV s^{-1} from −5 mV to 5 mV (vs. open-circuit potential) at 50% depth of discharge (DOD). The hydrogen diffusion coefficient was estimated by the potential-step method, and the experiment was tested in Gamry instrument at fully charged state with an overpotential of +600 mV and a discharge time of 4800 s. The electrodes were completely activated prior to the measurements mentioned above, and all of the electrochemical tests were performed at room temperature.

3. Results and discussion

3.1. Phase structure

Fig. 1 shows the XRD patterns of as-cast and annealed $La_{1.8}Ti_{0.2}MgNi_{8.9}Al_{0.1}$ alloys, and Table 1 lists the lattice parameters of the alloys. It can be seen from Fig. 1 and Table 1 that all the alloys consist of multiple phases, $La(Ni,Al)_5$ phase (space group P6/mmm) with the hexagonal $CaCu_5$-type structure and $LaMg_2Ni_9$ phase (space group R3m) with rhombohedral $PuNi_3$-type structure are the main phases. $LaNi_2$ phase (space group Fd-3m) with cubic $MgCu_2$-type structure disappears after annealing treatment. The lattice parameters of $La(Ni,Al)_5$ phase remain almost unchanged before and after annealing, and the cell volume of $LaMg_2Ni_9$ phase becomes smaller as annealing temperature reaches 1000 °C. After heat treatment, the most diffraction peaks became narrower and sharper due to the decrease of lattice defects [11] and homogenization of the composition [12].

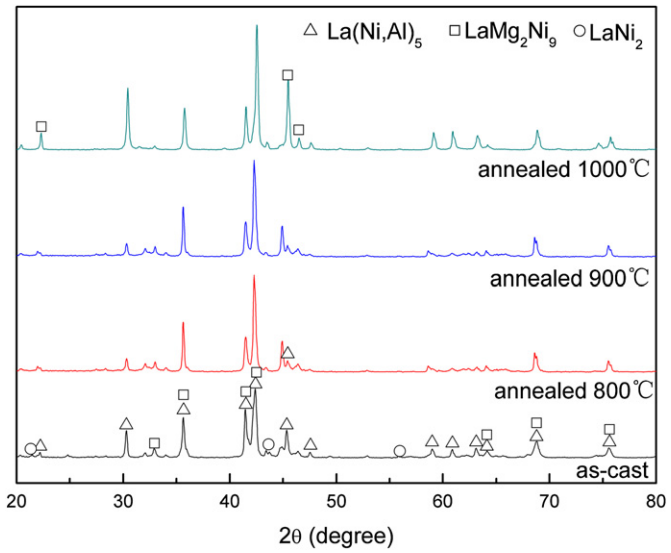

Fig. 1. XRD patterns of as-cast and annealed $La_{1.8}Ti_{0.2}MgNi_{8.9}Al_{0.1}$ alloys.

3.2. SEM–EDS analysis

Fig. 2 presents the surface micrographs of as-cast and annealed $La_{1.8}Ti_{0.2}MgNi_{8.9}Al_{0.1}$ alloys. As can be seen in Fig. 2, the distribution of metal phases becomes more homogenous after heat treatment, especially at 800 °C and 900 °C. Therefore, annealing treatment helps to improve the homogeneity, similar result is also found in our previous work on La–Ti–Mg–Ni alloys [10].

To identify the elemental composition in alloy, energy dispersive spectrometer (EDS) analysis is employed. Fig. 3 shows the EDS analysis patterns of as-cast and annealed $La_{1.8}Ti_{0.2}MgNi_{8.9}Al_{0.1}$ alloys, and the contents of all elements in the alloys are listed in the inset of Fig. 3. The component metals (La, Ti, Mg, Ni, Al) are dispersed in the alloy, indicating that Mg with low melting point has not been volatilized by annealing treatment. Referring to the phase composition of annealed alloys, it is found in Fig. 2 that besides the $La(Ni,Al)_5$ phase (the dark region denoted by A), the containing Mg phase, $LaMg_2Ni_9$ phase (the gray region denoted by B), is also present. This result is agreement with that of XRD analysis.

Table 1
The lattice parameters of as-cast and annealed $La_{1.8}Ti_{0.2}MgNi_{8.9}Al_{0.1}$ alloys.

Alloy	Phase	*a* (Å)	*b* (Å)	*c* (Å)	*V* (Å^3)
As-cast	$La(Ni,Al)_5$	5.02	5.02	4.01	87.36
	$LaMg_2Ni_9$	5.03	5.03	24.35	532.67
	$LaNi_2$	7.18	7.18	7.18	370.41
Annealed at 800 °C	$La(Ni,Al)_5$	5.02	5.02	4.01	87.83
	$LaMg_2Ni_9$	5.02	5.02	24.34	531.14
Annealed at 900 °C	$La(Ni,Al)_5$	5.03	5.03	4.01	87.71
	$LaMg_2Ni_9$	5.02	5.02	24.32	531.36
Annealed at 1000 °C	$La(Ni,Al)_5$	5.00	5.00	4.00	86.65
	$LaMg_2Ni_9$	4.92	4.92	23.87	501.03

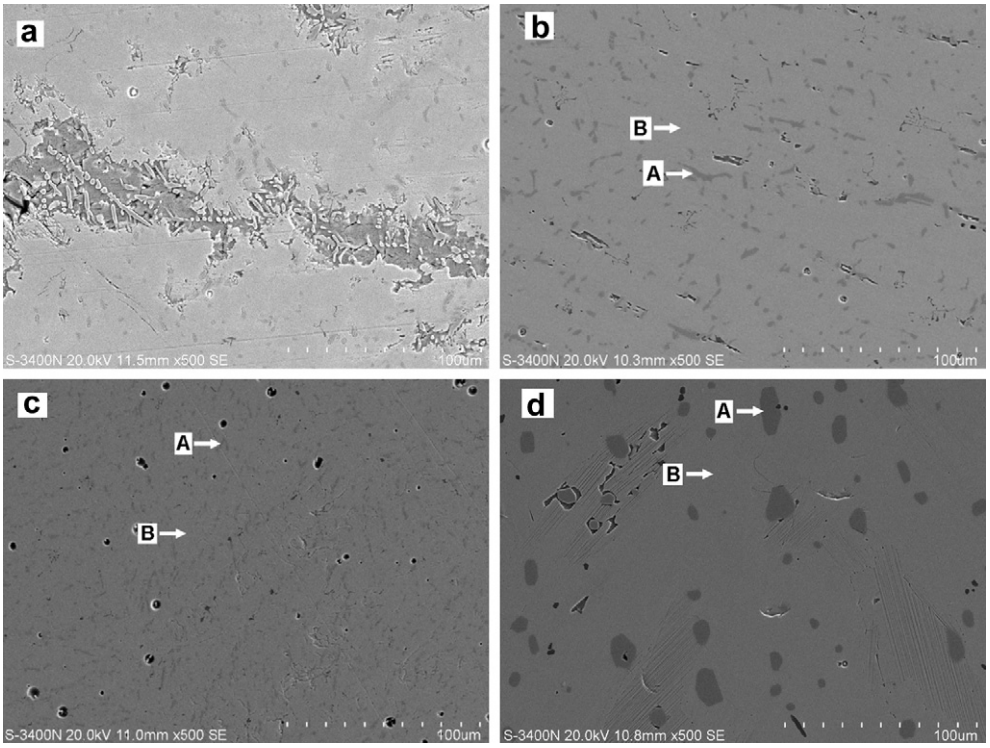

Fig. 2. SEM micrographs of $La_{1.8}Ti_{0.2}MgNi_{8.9}Al_{0.1}$ alloys, (a) as-cast; (b) annealed at 800 °C; (c) annealed at 900 °C; (d) annealed at 1000 °C.

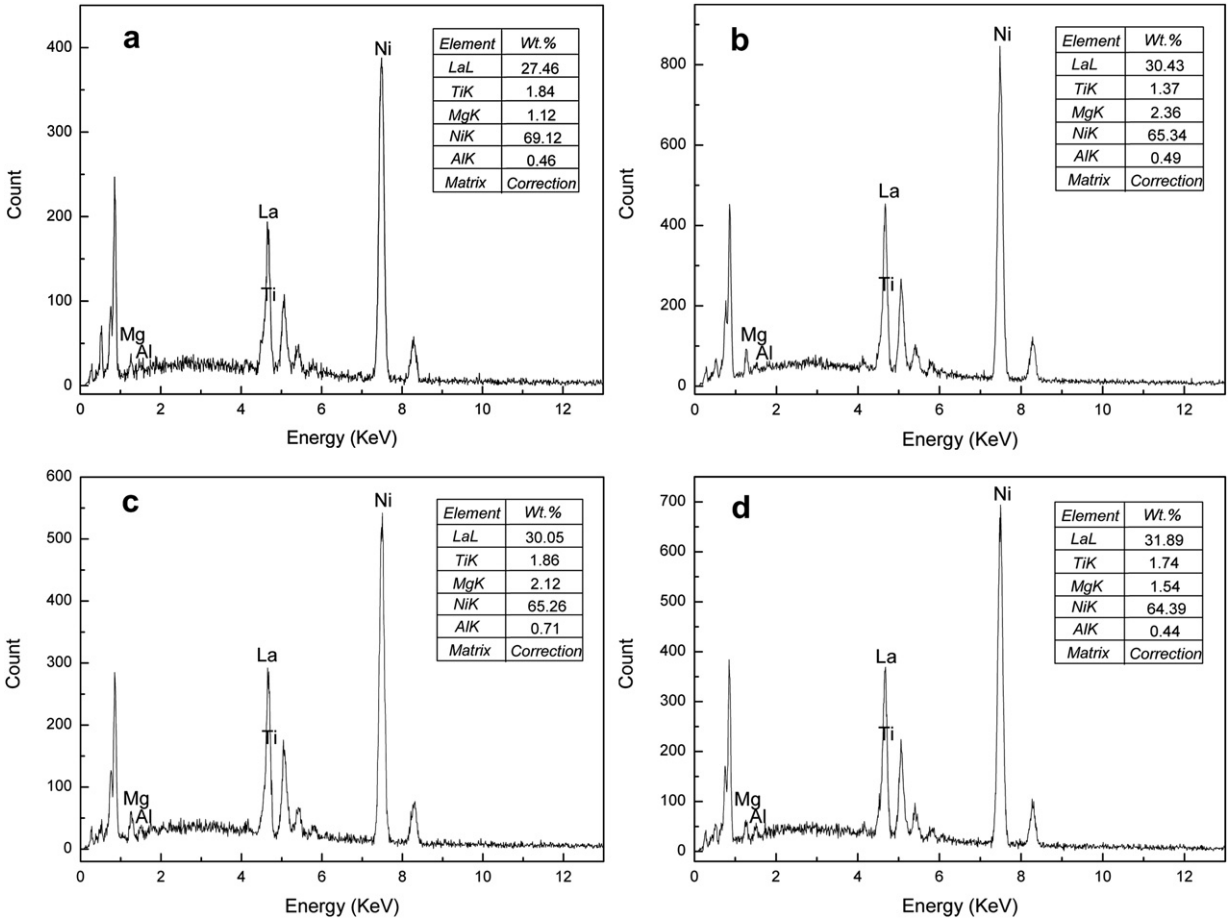

Fig. 3. EDS patterns of $La_{1.8}Ti_{0.2}MgNi_{8.9}Al_{0.1}$ alloys, (a) as-cast; (b) annealed at 800 °C; (c) annealed at 900 °C; (d) annealed at 1000 °C.

3.3. Charge/discharge performances

To further investigate the electrochemical properties of as-cast and annealed $La_{1.8}Ti_{0.2}MgNi_{8.9}Al_{0.1}$ alloy electrodes, the discharge capacity and cycling performance of the alloy electrodes are tested. Fig. 4 shows the cycling-lifetime curves of these alloy electrodes at 60% discharge capacity retention (ratio of discharge capacity to maximum discharge capacity). The experimental electrodes are fully activated within 2–4 cycles to reach the maximum discharge capacity (C_{max}) of 352.4 mAh g^{-1} (as-cast), 350.3 mAh g^{-1} (annealed at 800 °C), 358.4 mAh g^{-1} (annealed at 900 °C) and 359.5 mAh g^{-1} (annealed at 1000 °C), as shown in Table 2. Although the discharge capacity of $La_{1.8}Ti_{0.2}MgNi_{8.9}Al_{0.1}$ alloy electrode changes slightly before and after annealing, the cycling life has been improved significantly after annealing, especially at 800 °C and 900 °C. For instance, given the discharge capacity retention of 60%, the charge–discharge cycles (N_c) of $La_{1.8}Ti_{0.2}MgNi_{8.9}Al_{0.1}$ alloy electrodes increase from 51 (as-cast) to 106 (annealed at 800 °C), 160 (annealed at 900 °C) and 67 (annealed at 1000 °C) (Table 2). For as-cast alloy, the hydrogen-induced amorphization of highly stable $LaNi_2$ hydride [13,14] may be responsible for its faster capacity loss during charging and discharging. For annealed alloys, the higher compositional homogeneity (Figs. 1 and 2) for suppressing the pulverization and oxidation/corrosion of the alloy electrode in alkaline electrolyte [10,15,16], is thought to be beneficial to enhancing cycling stability. However, to high temperature (1000 °C), the positive impact of homogeneity on cycle life becomes limited due to the contraction of cell volume decreases anti-pulverization capability [17], thus, the cycling life of the alloy annealed at 1000 °C is only slightly better than the as-cast alloy and much worse than other annealed alloys.

The discharge voltage characteristic is an important property of alloy electrode. The longer and more horizontal the discharge voltage plateau is, the better the discharge characteristics the alloy electrode shows. Fig. 5 reveals the relationships between discharge capacity and discharge voltage of as-cast and annealed $La_{1.8}Ti_{0.2}MgNi_{8.9}Al_{0.1}$ alloy electrodes at an 80 mA g^{-1} discharge rate when they have reached the maximum discharge capacity after activation. It is noticed in Fig. 5 that the discharge voltage plateau becomes more horizontal after annealing treatment, moreover, annealed (900 °C and 1000 °C) alloys with relative high discharge capacity shows longer discharge voltage plateau. The results indicate that the discharge characteristics of $La_{1.8}Ti_{0.2}MgNi_{8.9}Al_{0.1}$ alloy electrode have been improved by annealing.

Table 2
Electrochemical performance of as-cast and annealed $La_{1.8}Ti_{0.2}MgNi_{8.9}Al_{0.1}$ alloy electrodes.

Alloy	C_{max} (mAh g^{-1})	N_c	HRD_{1000} (%)	I_0 (mA g^{-1})	D ($\times 10^{-10}$ cm^2 s^{-1})
As-cast	352.4	51	82.0	162.5	1.49
Annealed at 800 °C	350.3	106	86.0	257.7	1.84
Annealed at 900 °C	358.4	160	83.9	207.0	1.56
Annealed at 1000 °C	359.5	67	80.6	128.7	1.45

3.4. Electrochemical kinetic characteristics

High rate dischargeability (HRD) is very important for Ni/MH batteries used in power tool and hybrid electrical vehicle applications. Fig. 6 shows the HRD of as-cast and annealed $La_{1.8}Ti_{0.2}MgNi_{8.9}Al_{0.1}$ alloy electrodes at different discharge current density I_n (I_n = 80, 200, 400, 600, 800, 1000 mA g^{-1}). The HRD can be calculated according to the following equation:

$$HRD_n = \frac{C_n}{C_n + C_{80}} \times 100\% \quad (1)$$

where C_n is the discharge capacity at discharge current density I_n to a cut-off potential of −0.5 V vs. Hg/HgO reference electrode, C_{80} is the residual discharge capacity at discharge current density of 80 mA g^{-1} to a cut-off potential of −0.5 V vs. Hg/HgO reference electrode after the alloy electrode has been fully discharged at I_n. Obviously, except for the sample annealed at the highest temperature (1000 °C), the other annealed electrodes exhibit higher HRD than that of as-cast electrode. For example, at the discharge current density of 1000 mA g^{-1}, HRD_{1000} is 82.0%, 86.0%, 83.9% and 80.6% corresponding to as-cast alloy electrode, annealed alloy electrodes at 800 °C, 900 °C and 1000 °C, respectively (Table 2). The results indicate that suitable annealing temperature favors for the improvement of HRD characteristics, but if the annealing temperature is too high, the contraction of cell volume causes HRD to decrease [18]. In general, the HRD can represent the electrochemical kinetic performance of the alloy electrodes, and is considered to be mainly controlled by both the charge transfer rate

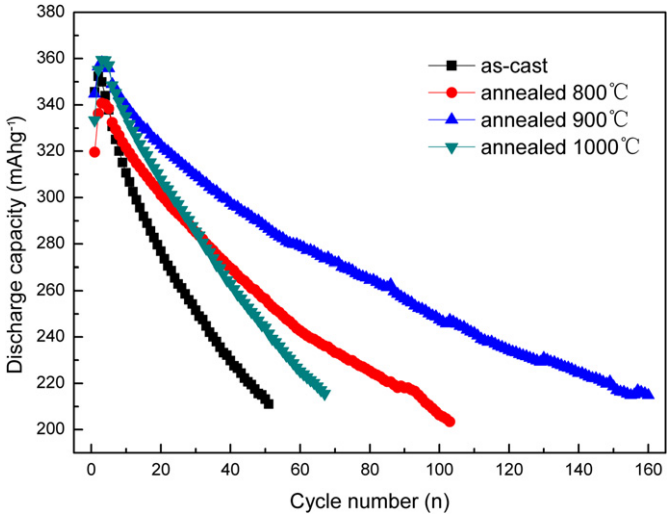

Fig. 4. Discharge cycling performance of as-cast and annealed $La_{1.8}Ti_{0.2}MgNi_{8.9}Al_{0.1}$ alloy electrodes.

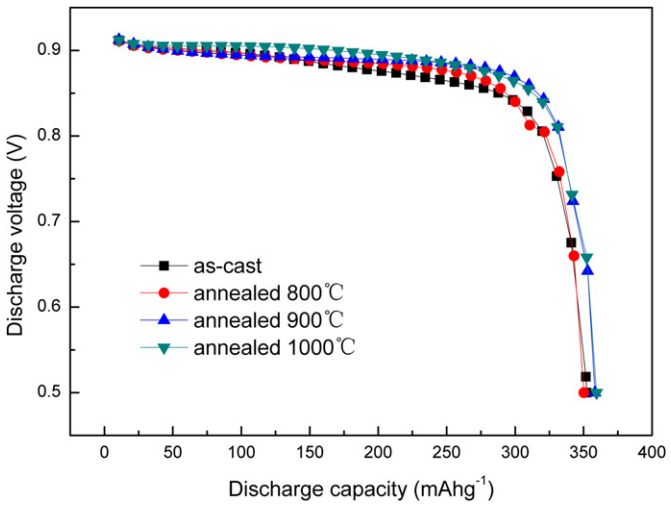

Fig. 5. Discharge curves of as-cast and annealed $La_{1.8}Ti_{0.2}MgNi_{8.9}Al_{0.1}$ alloy electrodes at 80 mA g^{-1} discharge rate.

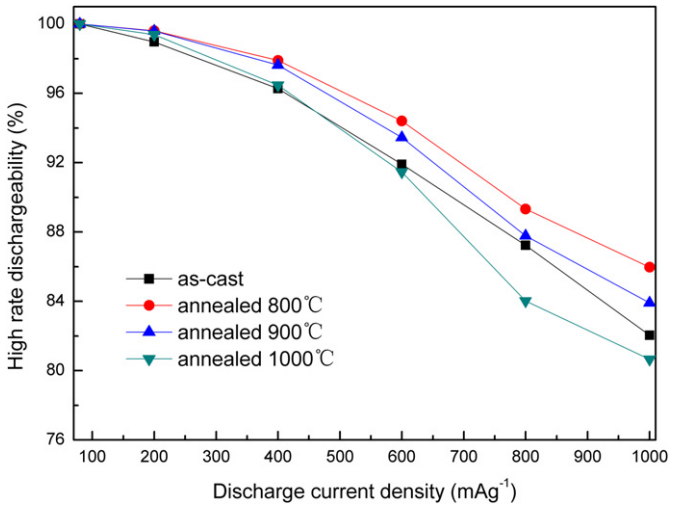

Fig. 6. High rate dischargeability of as-cast and annealed $La_{1.8}Ti_{0.2}MgNi_{8.9}Al_{0.1}$ alloy electrodes.

on the surface and the hydrogen diffusion rate in the bulk. To further make clear the variation tendency of the electrochemical kinetics, linear polarization and potential-step measurement are investigated.

Fig. 7 illustrates the linear polarization curves of as-cast and annealed $La_{1.8}Ti_{0.2}MgNi_{8.9}Al_{0.1}$ alloy electrodes at 50% DOD. Obviously, current and overpotential have a good linear dependence when the overpotential is changed within a small range (±5 mV). Generally, linear polarization process involves the hydrogen reduction and oxidation reactions at the surface layer of alloy powder. From the polarization curve, the exchange current density I_0, an important parameter for measuring the kinetics of electrochemical hydrogen reaction [19,20], can be calculated by the following equation [20]:

$$I_0 = \frac{jRT}{F\eta} \tag{2}$$

where I_0, j, R, T, F and η denote the exchange current density, the current density, the gas constant, the absolute temperature, the Faraday constant and the overpotential, respectively. Using linear least squares fitting method to find the slopes of related lines in Fig. 7, we can get the exchange current densities I_0 that are shown in Table 2. The exchange current density I_0 first increases from 162.5 mA g^{-1} (as-cast) to 257.7 mA g^{-1} (annealed at 800 °C) and 207.0 mA g^{-1} (annealed at 900 °C), and then decreases to 128.7 mA g^{-1} (annealed at 1000 °C). The variation of I_0 correlates well with the variation of HRD.

Hydrogen diffusion in the bulk of the alloy can be characterized by the hydrogen diffusion coefficient D determined from potential-step experiment. Measurements were performed on electrodes in fully charged state after cycling up to their maximum H-storage capacity. Fig. 8 shows the resulting current–time responses for as-cast and annealed $La_{1.8}Ti_{0.2}MgNi_{8.9}Al_{0.1}$ alloy electrodes. At sufficiently long discharge time, a slow and linear current decay controlled by the hydrogen diffusion velocity from inner to surface is observed. According to a spherical diffusion model [21], the hydrogen diffusion coefficient D can be calculated through the slope of the linear region of the corresponding plots, using the following equation [22]:

$$\log i = \log\left(\frac{6FD}{da^2}(C_0 - C_S)\right) - \frac{\pi^2 D}{2.303a^2}t \tag{3}$$

in which i is the diffusion current density, F is the Faraday constant, D is the hydrogen diffusion coefficient, d is the density of the material, a is the average particle radius (assumed as spherical), C_0 is the initial hydrogen concentration in the bulk (considered as uniform), C_S is the hydrogen concentration at the electrode surface (considered as constant) and t is the discharge time. Although the assumed sphere-like particles in experiments is not satisfied completely, the errors with this assumption were found not to be serious [21], so that the spherical particles are appropriate for hydrogen diffusion coefficient calculation [16,23,24]. Setting the average particle radius as a = 18.8 μm, the hydrogen diffusion coefficient D is calculated by the above equation and tabulated in Table 2. It can be seen that the hydrogen diffusion coefficient D changes from 1.49×10^{-10} cm^2 s^{-1} (as-cast), to 1.84×10^{-10} cm^2 s^{-1} (annealed at 800 °C), 1.56×10^{-10} cm^2 s^{-1} (annealed at 900 °C) and 1.45×10^{-10} cm^2 s^{-1} (annealed at 1000 °C). The variation of hydrogen diffusion coefficient is in good agreement with that of HRD.

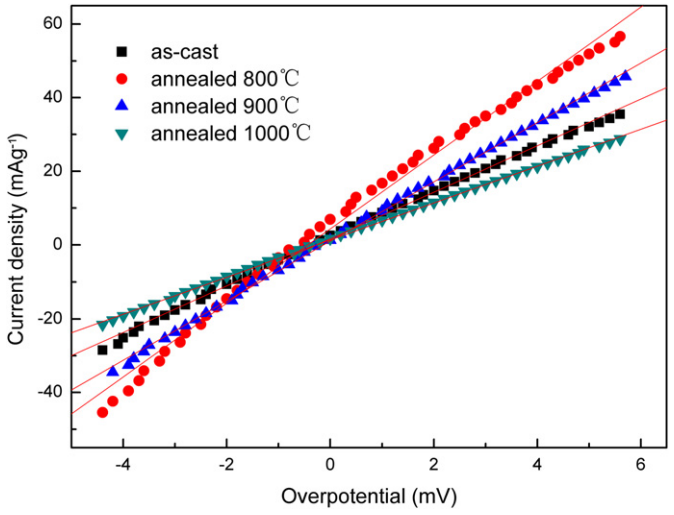

Fig. 7. Linear polarization curves of as-cast and annealed $La_{1.8}Ti_{0.2}MgNi_{8.9}Al_{0.1}$ alloy electrodes at 50% DOD.

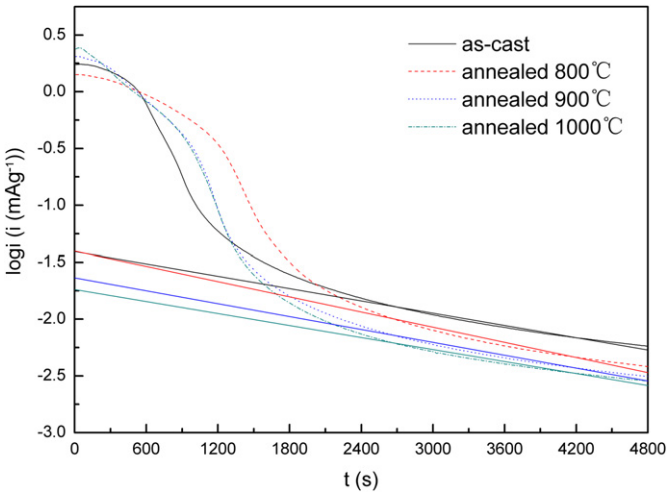

Fig. 8. Semilogarithmic curves of anodic current vs. time responses of as-cast and annealed $La_{1.8}Ti_{0.2}MgNi_{8.9}Al_{0.1}$ alloy electrodes at 100% DOD.

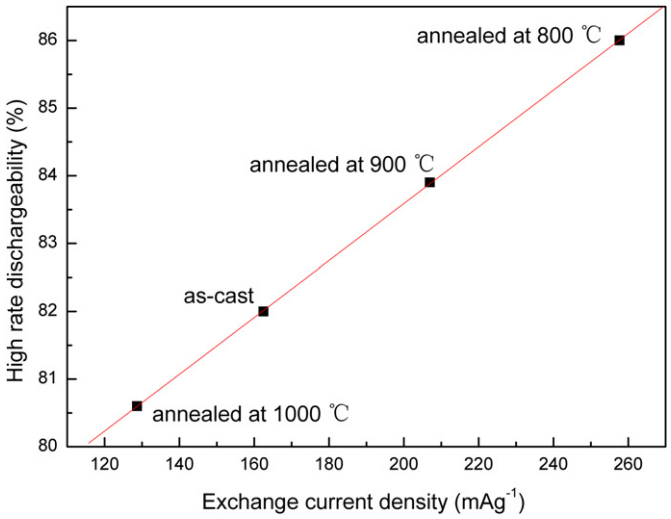

Fig. 9. High rate dischargeability at 1000 mA g^{-1} as a function of exchange current density for as-cast and annealed $La_{1.8}Ti_{0.2}MgNi_{8.9}Al_{0.1}$ alloy electrodes.

As mentioned above, HRD is influenced by the electrochemical kinetics on the alloy surface and the diffusion rate of hydrogen atom in the bulk. Iwakura et al. [25] have shown that, if the electrochemical reaction on the surface is the rate-determining factor, a linear dependence of the high rate dischargeability on the exchange current density should be observed. In contrast, if the diffusion of hydrogen in the bulk is the rate-determining factor, the high rate dischargeability should be constant, irrespective of exchange current density. Fig. 9 shows the high rate dischargeability HRD_{1000} as a function of exchange current density I_0 for as-cast and annealed $La_{1.8}Ti_{0.2}MgNi_{8.9}Al_{0.1}$ alloy electrodes. Obviously, there is a good linear relationship between HRD_{1000} and I_0, which indicates that the HRD is essentially controlled by the charge–transfer reaction at the surface of the alloy electrodes.

Considering the cycling stability shown in Fig. 4, discharge behavior illustrated in Fig. 5 and electrochemical kinetic described in Figs. 6–8, it can be concluded that suitable annealing treatment (800 °C and 900 °C) favors for the improvement of electrochemical performance of $La_{1.8}Ti_{0.2}MgNi_{8.9}Al_{0.1}$ alloy electrodes, and the most appropriate annealing temperature for the alloy studied is 900 °C.

4. Conclusions

In order to improve the electrochemical properties of $La_{1.8}Ti_{0.2}MgNi_{8.9}Al_{0.1}$ alloy, annealing treatment was carried out. The effects of annealing on the electrochemical properties of as-cast and annealed $La_{1.8}Ti_{0.2}MgNi_{8.9}Al_{0.1}$ alloys are investigated by means of XRD, SEM–EDS and electrochemical measurement. The results show the experimental alloys mainly consist of two phases namely $La(Ni,Al)_5$ and $LaMg_2Ni_9$. The lattice parameters of $La(Ni,Al)_5$ phase remain almost unchanged before and after annealing, and the cell volume of $LaMg_2Ni_9$ phase contract at 1000 °C. Annealing not only leads to the disappearance of $LaNi_2$ phase, but also improves the compositional homogeneity, which favors for the improvement of cycling stability especially at 800 °C and 900 °C. Suitable annealing treatment (800 °C and 900 °C) can increase both the charge transfer rate at the surface and the hydrogen diffusion rate in the bulk, and consequently, enhances the HRD. $La_{1.8}Ti_{0.2}MgNi_{8.9}Al_{0.1}$ alloy annealed at 900 °C exhibits good overall electrochemical performance, with the maximum discharge capacity of 358.4 mAh g^{-1}, the HRD_{1000} of 83.9%, and the discharge capacity retention of 60% after 160 charge–discharge cycles.

Acknowledgments

This work was supported by the National Natural Science Foundation of China (51071054), the Natural Science Foundation of Guangxi (2010GXNSFD013004, 2012GXNSFBA053149), the Foundation of Key Laboratory of National Education Ministry for Nonferrous Metals and Materials Processing Technology (GXKFJ09-15), the Guangxi University Program for Science and Technology Research (XBZ110379).

References

[1] K. Kadir, T. Sakai, I. Uehara, J. Alloy. Compd. 257 (1997) 115–121.
[2] K. Kadir, T. Sakai, I. Uehara, J. Alloy. Compd. 302 (2000) 112–117.
[3] T. Kohno, H. Yoshida, F. Kawashima, T. Inaba, I. Sakai, M. Yamamoto, M. Kanda, J. Alloy. Compd. 311 (2000) L5–L7.
[4] B.W. Li, Y.H. Zhang, Z.W. Wu, Y.C. Shi, Z.G. Pang, X.L. Wang, Int. J. Hydrog. Energy 33 (2008) 141–148.
[5] Y. Zhao, M.X. Gao, Y.F. Liu, L. Huang, H.G. Pan, J. Alloy. Compd. 496 (2010) 454–461.
[6] T. Sakai, H. Miyamura, N. Kuriyama, H. Ishikawa, I. Uehara, Z. Phys. Chem. Bd. 183 (1994) 333–346.
[7] H.G. Pan, N. Chen, M.X. Gao, R. Li, Y.Q. Lei, Q.D. Wang, J. Alloy. Compd. 397 (2005) 306–312.
[8] F.L. Zhang, Y.C. Luo, J.P. Chen, R.X. Yan, L. Kang, J.H. Chen, J. Power Sources 150 (2005) 247–254.
[9] T.Z. Huang, J.T. Han, Y.H. Zhang, J.M. Yu, G.X. Sun, H. Ren, X.X. Yuan, J. Power Sources 196 (2011) 9585–9589.
[10] W.Q. Jiang, Z.Q. Lan, W.L. Wei, Y.X. Liu, J. Guo, Int. J. Hydrog. Energy 35 (2010) 11016–11024.
[11] K. Nomura, H. Uruno, S. Ono, H. Shinozuka, S. Suda, J. Less-Common Met. 107 (1985) 221–230.
[12] Y. Nakamura, H. Nakamura, S. Fujitani, I. Yonezu, J. Alloy. Compd. 210 (1994) 299–303.
[13] H. Miyamura, T. Sakai, K. Oguro, A. Kato, H. Ishikawa, J. Less-common Met. 146 (1989) 197–203.
[14] H. Miyamura, N. Kuriyama, T. Sakai, K. Oguro, A. Kato, H. Ishikawa, T. Iwasaki, J. Less-common Met. 172–174 (1991) 1205–1210.
[15] H.G. Pan, Y.F. Liu, M.X. Gao, Y.F. Zhu, Y.Q. Lei, Q.D. Wang, Int. J. Hydrog. Energy 28 (2003) 113–117.
[16] M. He, H.G. Pan, S.C. Zhang, N. Chen, R. Li, M.X. Gao, Int. J. Hydrog. Energy 32 (2007) 3387–3394.
[17] Y.H. Zhang, B.W. Li, H.P. Ren, Y. Cai, X.P. Dong, X.L. Wang, J. Alloy. Compd. 458 (2008) 340–345.
[18] S. Ma, M.X. Gao, R. Li, H.G. Pan, Y.Q. Lei, J. Alloy. Compd. 457 (2008) 457–464.
[19] H. Yayama, K. Kuroki, K. Hirakawa, A. Tomokiyo, Jpn. J. Appl. Phys. 23 (1984) 1619–1623.
[20] P.H.L. Notten, P. Hokkeling, J. Electrochem. Soc. 138 (1991) 1877–1885.
[21] H. Ura, T. Nishina, I. Uchida, J. Electroanal. Chem. 396 (1995) 169–173.
[22] G. Zheng, B.N. Popov, R.E. White, J. Electrochem. Soc. 142 (1995) 2695–2698.
[23] T. Nishina, H. Ura, I. Uchida, J. Electrochem. Soc. 144 (1997) 1273–1277.
[24] Y.F. Liu, H.G. Pan, M.X. Gao, Y.F. Zhu, Y.Q. Lei, Q.D. Wang, Electrochim. Acta 49 (2004) 545–555.
[25] C. Iwakura, T. Oura, H. Inoue, M. Matsuoka, Electrochim. Acta 41 (1996) 117–121.